GIANTLEAP

Diagnostic methods for automotive fuel cell systems

Ivan Pivac, Gojmir Radica, Frano Barbir (FESB), Djedjiga Benouioua, Fabien Harel, Denis Candusso (UFC/IFSTTAR/FCLAB)

Quality Assurance: Daniel Hissel (UFC)

Project acronym:	GIANTLEAP

Project acronym: GIANTLEAP

Project title: Giantleap Improves Automation of Non-polluting Transportation with Lifetime Extension of Automotive PEM fuel cells

Project number: 700101

Document date: December 29, 2017

Due date: October 31, 2017

Keywords: Catalyst degradation, Accelerated Stress Test, Electrochemical Impedance Spectroscopy, Low Frequency Intercept, Balance-of-Plant Components Ageing, Air compressor

Abstract: The deliverable presents the obtained measurement and analysis results of the accelerated ageing test protocols and different diagnostic methods (polarization curves, electrochemical impedance spectroscopy, cyclic voltammetry, linear sweep voltammetry), which were performed at FESB on an already conditioned 50 cm2 (single) fuel cell provided by ElringKlinger to verify the available data and gather any missing data points. In collaboration with SINTEF, an idea of new, time-efficient, direct measurement approach of low-frequency intercept in the impedance spectrum, as the quick indicator of catalyst degradation which can provide the possibility to determine the current state of the fuel cell from just one parameter value, is also briefly given at the end of this deliverable, which is very promising for the future implementation in the fuel cell control system, but the direct identification approach will be further explored. University of Franche-Comté /FCLab contribution in WP1 is to develop diagnostic strategies to ensure the FC System Air Line (FCSAL) State-of-Health (SoH) monitoring. Three diagnostic strategies are implemented and validated on data gathered from previous FC LAB projects. The diagnostic approaches are based on data-driven diagnostic techniques – algorithms are fed by physical signals such as stack voltage and pressure signal measurements. Guidelines for implementation of each strategy in the Giantleap project on data to be recorded on FCEB prototype from Bosch are provided.

Revision History

| Date	Description	Author
04.12.2017	First draft	Frano Barbir (FESB)
22.12.2017	Quality Assurance	Daniel Hissel (UFC)
28.12.2017	Final version	Frano Barbir
29.12.2017	Last typographical corrections	Federico Zenith (SINTEF)

Table of Contents

1 Introduction

Durability is one of the main shortcomings in state-of-the-art automotive fuel cell systems, because performance of proton exchange membrane (PEM) fuel cells degrades over time, which limits a faster commercialization of this zero-emission power technology. Many researchers worldwide are devoted to find a better understanding of degradation causes and mechanisms, with early detection of the degradation symptoms. However, diagnostics of fuel cell degradation should not only detect the symptoms, as early as possible, but also identify the causes and/or mechanisms, if it is possible, so that corrective actions could be taken [1]. There are several degradation mechanisms, typical for automotive applications, such as: degradation of the catalyst layer caused by carbon corrosion due to frequent starts and stops (air fuel front), loss of catalyst active area caused by platinum dissolution and sintering due to frequent voltage cycling, loss of catalyst active area due to adsorption of contaminants from the inlet gases, mechanical degradation due to thermal and humidity cycling induced by the load profile as well as by the environment in which the vehicle operates. In project deliverable D1.3, FESB has selected the most relevant degradation mechanisms in fuel cells for automotive systems, and the collected data was there used to rank and quantify each identified degradation pattern and devise appropriate accelerated testing techniques. Hence, the loss of catalyst active area caused by platinum dissolution and sintering due to frequent voltage cycling was selected here as the target for the laboratory experiments as the most relevant for the fuel cell systems in automotive application.

The aim of this deliverable is to present ageing test protocol, characterization and measurement techniques and their periodicity during the accelerated degradation test of the automotive fuel cell system to estimate the current state of fuel cell systems. The deliverable presents the obtained measurement and analysis results of the accelerated ageing test protocols and different diagnostic methods (polarization curves, electrochemical impedance spectroscopy, cyclic voltammetry, linear sweep voltammetry), which were performed at FESB's Laboratory for New Energy Technologies on an already conditioned 50 cm^2 (single) fuel cell provided by ElringKlinger to verify the available data and gather any missing data points. In collaboration with SINTEF, an idea of new time-efficient measurement approach of low-frequency intercept in the impedance spectrum, as the quick indicator of catalyst degradation which can provide the possibility to determine the current state of the fuel cell from just one parameter value, is also briefly given at the end of this deliverable, which is very promising for the future implementation in the fuel cell control system, but the direct identification approach will be further explored. In addition, this deliverable presents three diagnostic strategies being developed by UFC to ensure the fuel cell system air supply State-of-Health (SoH) monitoring.

2 Accelerated degradation tests and diagnostics

In order to correlate with the findings from the previous FCHJU project SAPPHIRE, an accelerated stress test (AST) has been performed on 50 cm^2 active area single PEM fuel cell from ElringKlinger (EK), using the same MEA configuration as it will be used in the full-size stacks (Figure 1). This water-cooled single cell was tested in co-flow configuration. It was exposed to an accelerated stress test for catalyst degradation during which several standard laboratory diagnostic procedures were periodically performed in order to monitor degradation. These diagnostic methods include polarization curves, electrochemical impedance spectroscopy (EIS), cyclic voltammetry (CV), and linear sweep voltammetry (LSV).
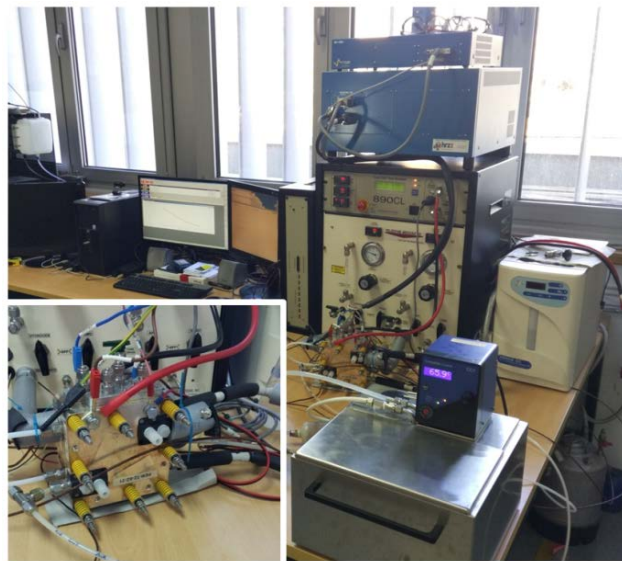
Figure 1: Experimental setup with investigated ElringKlinger's single PEM fuel cell.

The AST designed to target electrocatalyst degradation, involves 40 seconds long potential cycling profile (Figure 2) between voltages of 0.6 V for 10 s and 0.9 V for 30 s, which is slightly modified version of the U.S. Department of Energy (DoE) recommended AST protocol for electrocatalyst degradation [2]. Instead of cycling between 0.7 V and 0.9 V, cycling was conducted between 0.6 V and 0.9 V, in order to speed-up the degradation process. Similar test protocols were used in the SAPPHIRE. The voltage was imposed on the cell at 65 °C and 0.5 bar(g) via an external instrument (BioLogic SP-150 potentiostat/galvanostat) as the cell was in a non-operating ("driven") mode, i.e. nitrogen was used on the cathode and hydrogen on the anode side with constant flows of 0.4 SLPM and inlet relative humidities (RH) of 100% (dew point of 65 °C). Because the tubing material at the test station was limited to a maximum temperature of 80 °C, all the temperatures in these tests were limited to 65 °C in order to reduce the potential impact of some unwanted dissolved chemical pipe elements and compounds on electrocatalyst degradation in the fuel cell. However, further degradation testing is also planned to run at 80 °C for further comparison with these results, because catalyst degradation is expected to be more pronounced at higher temperatures.
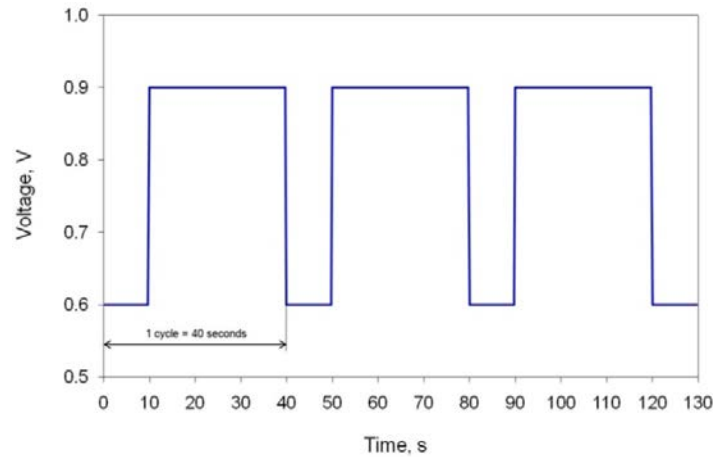
Figure 2: Potential cycling profile in accelerated stress test for electrocatalyst degradation.

Cell's diagnostics were performed periodically at the beginning of life (BoL), and then after 1000, 3000, 5000 and 10000 cycles. Additionally, CVs and LSVs were also performed after 100, 300 and 500 cycles as recommended by the DOE AST protocol. In order to investigate the reversibility phenomena of catalyst layer degradation, i.e. rejuvenation of the fuel cell, the experiment was stopped after 5000 cycles (around 56 h) for 4 days as the intentional recovery period, and then is continued for another 5000 cycles with another intentional recovery period after 10000 cycles for 4 days. Additionally, the same diagnostic measurements were repeated 6 months later on the same EK's fuel cell, which was lying unused and closed during these 6 months. However, analysis of these results of the reversible degradation will be in our further project deliverable D1.5, as a part of the WP1 Task 1.5.

2.1 Results of Accelerated Stress Test

2.1.1 Polarization curves

Polarization curves were recorded in descending and ascending direction with the rest time of 5 min at each point. Stoichiometries of anode and cathode were 2 and 4 respectively, while the relative humidity (RH) was set to 83.4% for both reactants (dew point of 61 °C). The resulting averaged polarization curves obtained during the AST are shown in Figure 3.
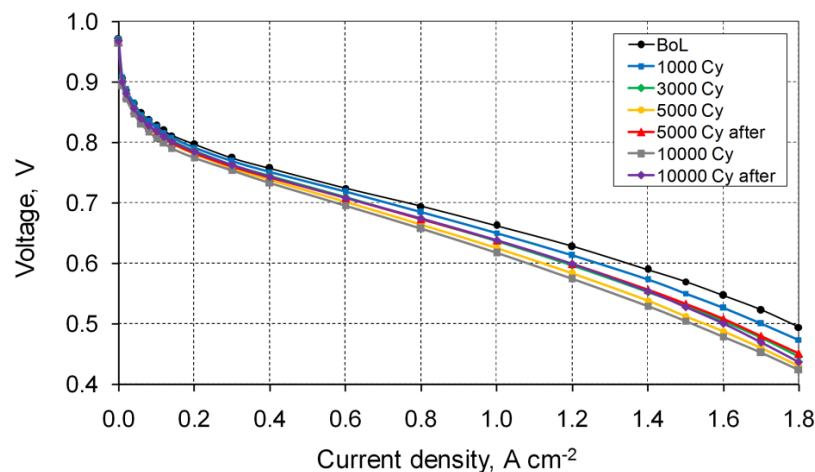

Figure 3: Comparison of measured polarization curves during the accelerated stress test.

From the plotted polarization curves degradation is noticeable, but it may be quantified if the cell potential at different current densities is plotted vs. time or vs. number of cycles as shown in Figure 4. Degradation is more pronounced at higher current densities. Also, what is noticeable is some recovery after 5000 and 10000 cycles, which means that not all of exhibited degradation is permanent. More efforts on elucidating this phenomenon will be applied in the next phase of this project.
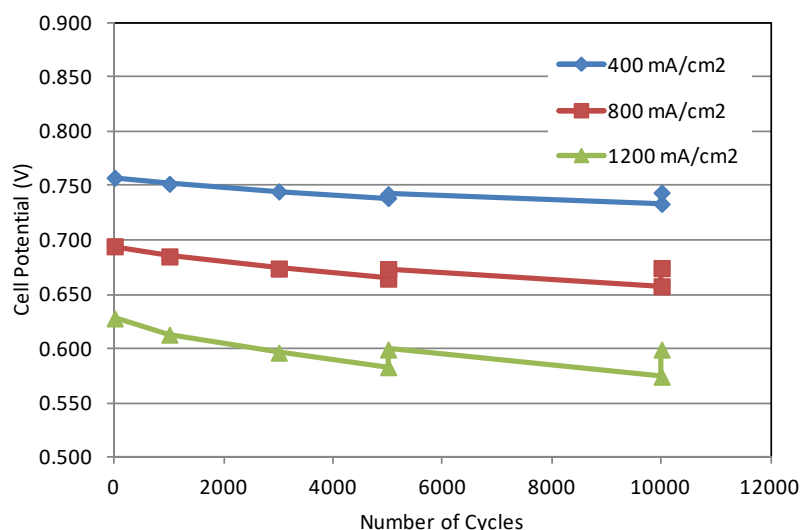

Figure 4: Degradation at different current densities during the accelerated stress test.

2.1.2   Cyclic voltammetry

Cycling voltammetry (CV) measurements were recorded with the anode as a counter and a reference electrode, and the cathode as a working electrode. Constant flows of 0.4 SLPM and 100% RH (dew point 65 °C) hydrogen and nitrogen were used on anode and cathode, respectively. Five cycles (between 0.05 and 0.6 V) with a sweep rate of 50 mV s^{-1} were conducted with the last one recorded as representative.

The results of the CV measurements during the AST are shown in Figure 13. The purpose of CVs was to obtain the change of the electrochemical active surface area (ECSA) during the AST. This was obtained by integrating the surface under the part of the curve corresponding to H2 electrodesorption (the "upper" part of the curve) and subtracting the contribution of the capacitive charging of the double layer. The obtained surface area represents the amount of charge exchanged during the hydrogen desorption and should be proportional to the platinum active area. The exact ECSA (cm_{Pt}^2 cm^{-2}) was calculated by dividing this area by the Coulombic charge required to desorb hydrogen from a clean Pt surface (0.21 mC cm_{Pt}^{-2}) and the CV sweep rate (50 mV s^{-1}). The calculated ECSA values and their loss in percentage during the AST are also given in Figure 5.

As intended, CVs indicated a loss of the ECSA probably caused by platinum dissolution due to intentional frequent voltage cycling during the AST, but it is still under the target of the DOE protocol for CV (i.e. at least 40% loss of initial active area) and it is much smaller loss of ECSA during the AST than in some previous studies at FESB [1]. During the first 1000 cycles, ECSA was practically unchanged. After 10000 cycles, it was reduced to 78.1% of the original area (Figure 5). The loss of the

ECSA apparently resulted in structural changes within the catalyst layer, as the increase in resistance and in mass transport suggests from the subsequent analyses.
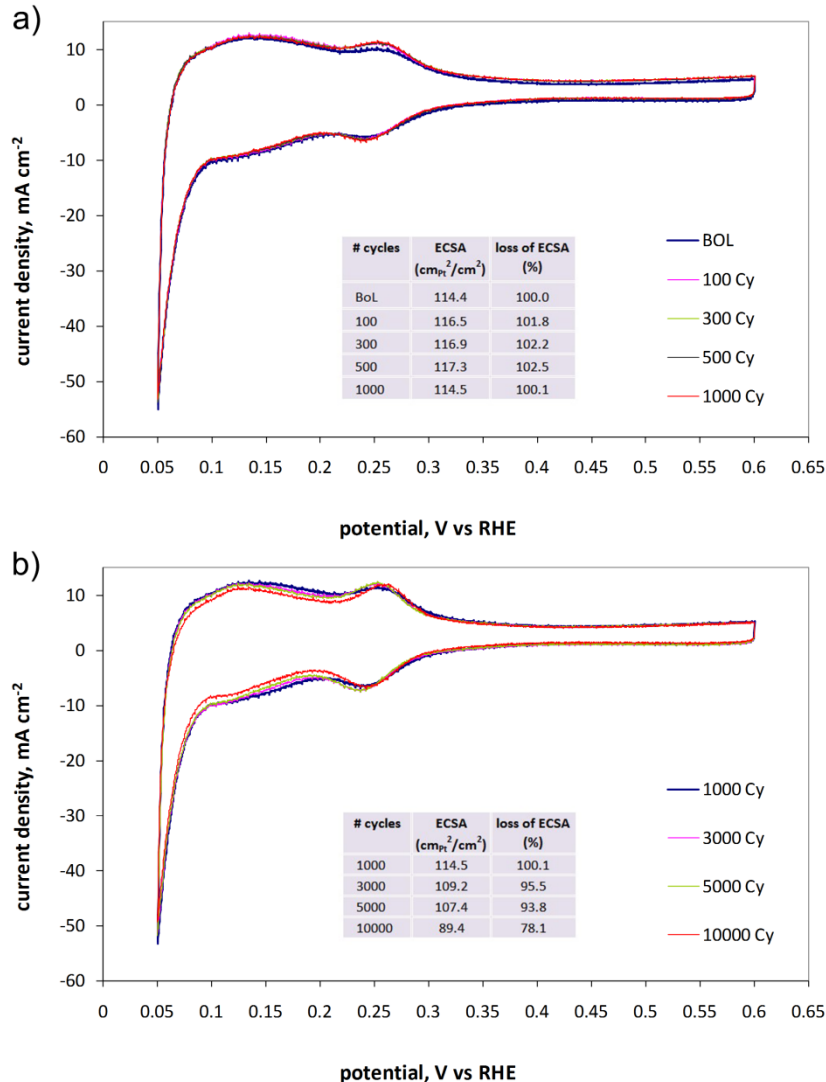

Figure 5: Comparison of cyclic voltammograms with the loss of ECSA during the accelerated stress test: a) from BoL to 1000 cycles; b) from 1000 to 10000 cycles.

2.1.3 Linear sweep voltammetry

Linear sweep voltammetry (LSV) measurements were conducted with all the parameters same as with the CV but with a sweep rate of 2 mV s^{-1} between 0.1 and 0.5 V. The results of the LSV measurements (shown in Figure 6) indicated that hydrogen crossover, expectedly, did not change significantly during the AST. It was around 2.6 mA cm^{-2}, with a slight tendency to decrease after 1000 cycles to 10000 cycles (Figure 14b). Because this AST targeted degradation of the catalyst, there is no reason for hydrogen crossover to change significantly.
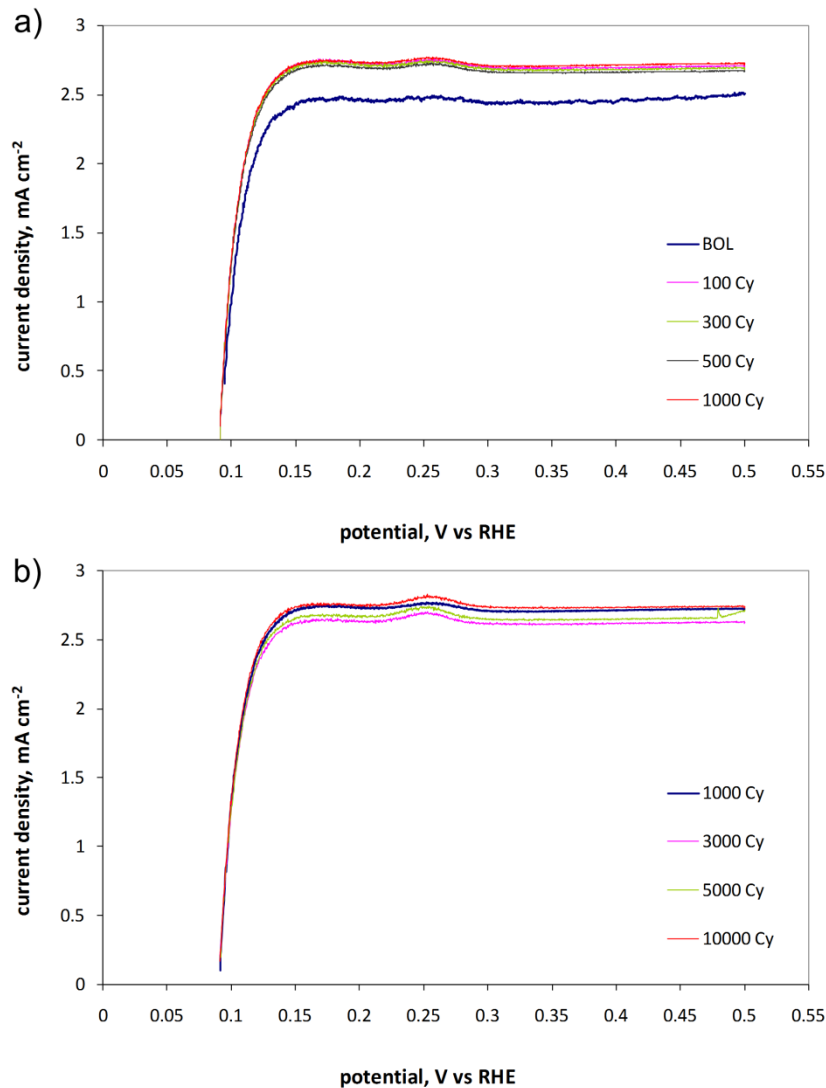
Figure 6: Comparison of linear sweep voltammograms during the accelerated stress test: a) from BoL to 1000 cycles; b) from 1000 to 10000 cycles.

2.1.4 Electrochemical impedance spectroscopy

The electrochemical impedance spectroscopy (EIS) measurements were conducted in a galvanostatic mode in the frequency range from 3.981 kHz to 10 mHz with AC signal amplitude of 10% of the DC current. A Scribner Associates 890CL Teledyne Medusa fuel cell test station, which contains both an electronic load and a frequency response analyzer (FRA) for full range impedance measurements up to 10 kHz, was used for the experiments. Each scan took around thirty minutes with additional five minutes of stabilization phase prior to each testing. In order to obtain the evolution of the Nyquist impedance plots along the polarization curve during the AST the series of three EIS measurements at current density of 0.3, 0.6 and 1.2 A cm^{-2} were measured (Figure 7), with reactants inlet RH of 83.4% (dew point of 61 °C) and constant stoichiometry of 4.0/2.0. The resulting Nyquist plots obtained at different current densities during the AST are shown in Figure 8-Figure 10.

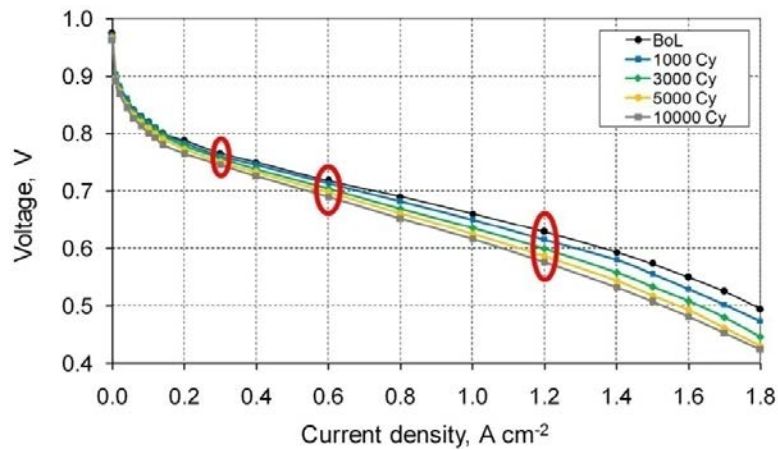*Figure 7: Comparison of measured polarization curves in descending direction during the accelerated stress test with red-marked EIS measurement points.*
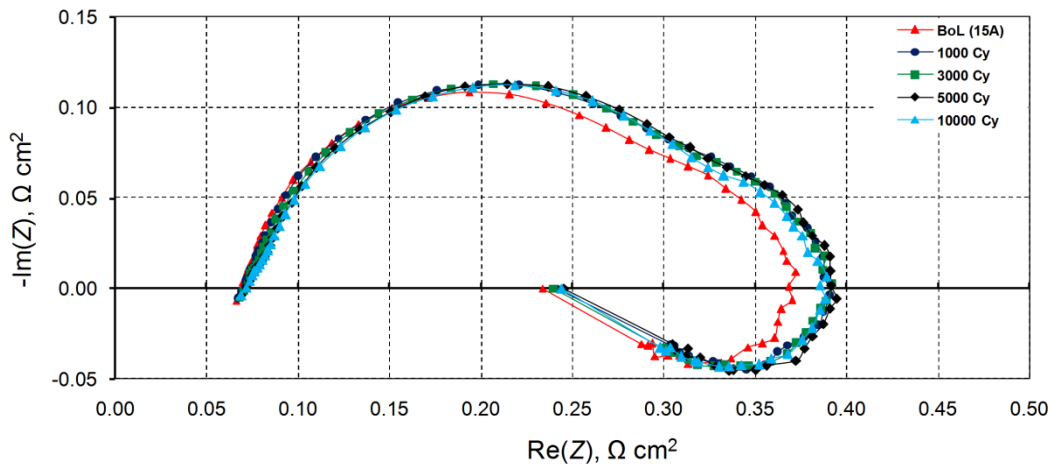

Figure 8: Comparison of measured impedance spectra at 0.3 A cm⁻² obtained during the accelerated stress test.
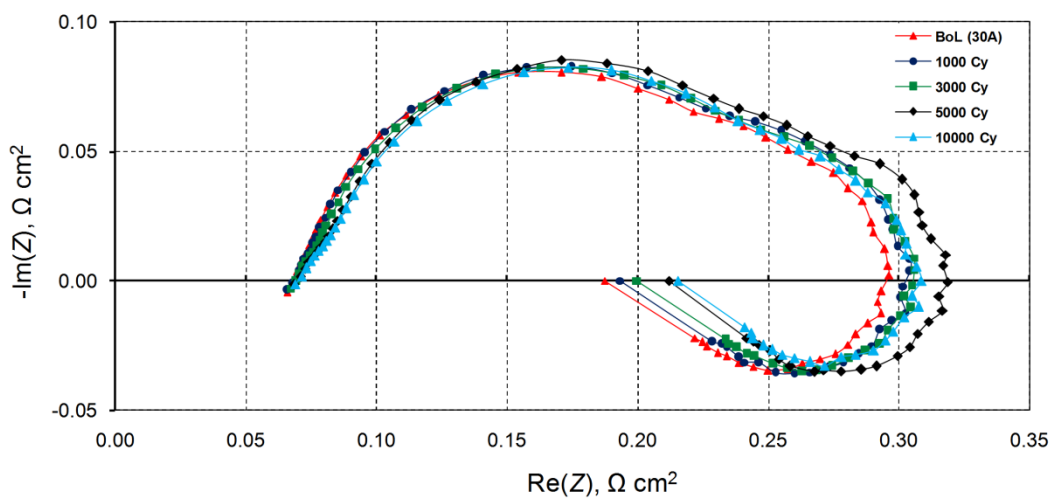

Figure 9: Comparison of measured impedance spectra at 0.6 A cm⁻² obtained during the accelerated stress test.
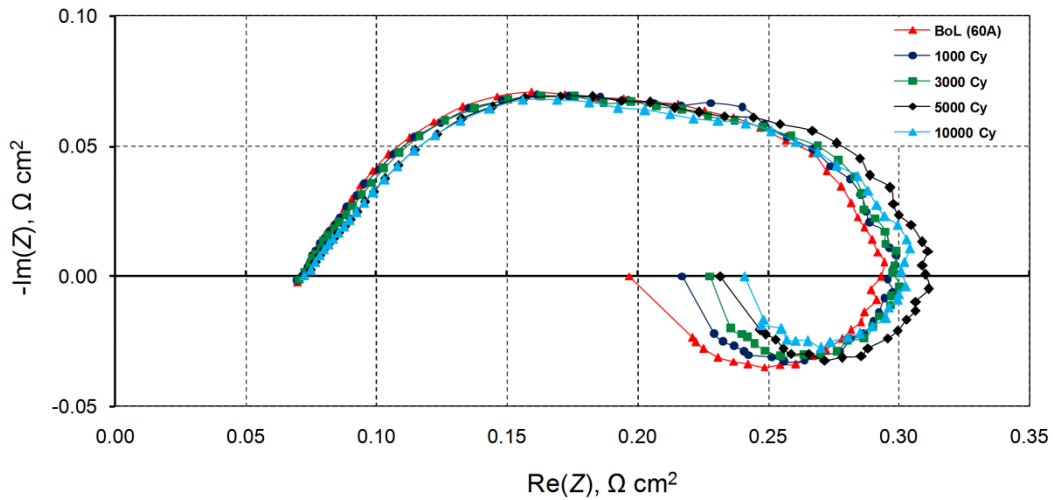
Diagnostic methods for automotive fuel cell systems

Figure 10: Comparison of measured impedance spectra at 1.2 A cm^{-2} obtained during the accelerated stress test.

From the results of the EIS measurements taken during the AST at three different current densities, catalyst degradation during the first 5000 cycles is visible in every case, which is even more clearly displayed in Figure 9. However, due to rejuvenation of the fuel cell during the intentional recovery period of 4 days between 5000 and 10000 cycles, impedance spectra in Figure 8-Figure 10 also show some reversibility, i.e. reduction/improvement of the impedance curves from 5000 to 10000 cycles. Therefore, comparison of the measured impedance spectra at different current densities in Figure 11 is given at the beginning of life (BoL) and after the first 5000 cycles of the accelerated stress test.
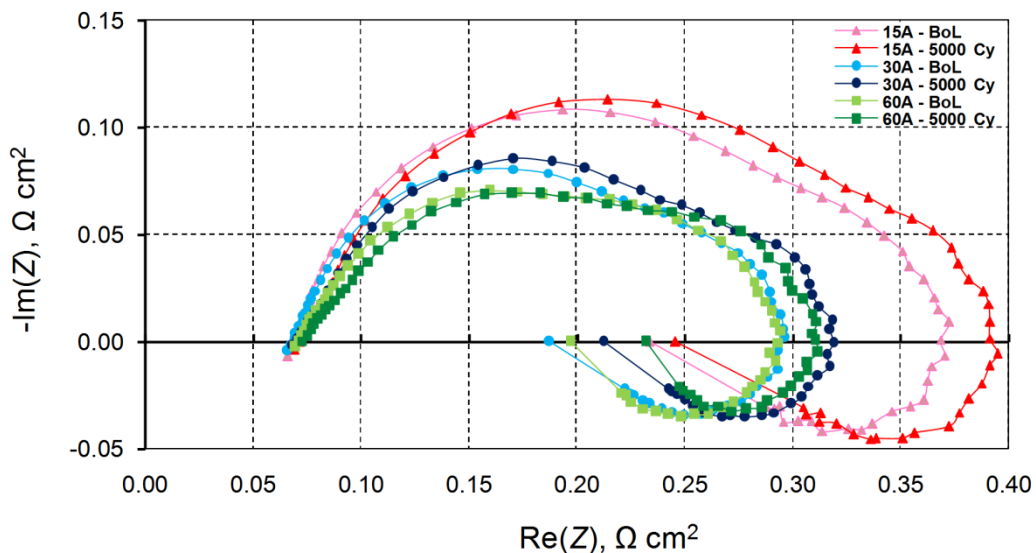
Figure 11: Comparison of measured impedance spectra at different current densities obtained at the beginning of life (BoL) and after 5000 cycles of accelerated stress test.

The semicircles' high-frequency branches are more tilted/distorted with degradation, indicating an increase in the catalyst layer (CL) ionic resistance, while the low-frequency loops, representing mass transport losses, are getting bigger. As a result, the rightmost real-axis intercept on the Nyquist diagram around 0.5 Hz or lower (the point with maximum real impedance and the highest resistive

losses), defined here as the total resistance (Total R), increased most significantly, while the membrane resistance (the leftmost real-axis intercept at high frequencies) showed a slight increase, as the EIS measurements were performed with not fully-hydrated reactants (83.4% RH). Obviously, there is a mixture of increase in activation losses (related to the loss of the cathode electrochemical active surface area, ECSA) and mass transport losses. This concurs also with the findings (at least qualitatively) of cycling voltammetry and the polarization change curves analysis (subsection 2.2.1).

2.2   Analyses of Accelerated Stress Test Results

2.2.1   Polarization change curves

Polarization change curves, defined as a difference between the polarization curve at the beginning of life (BoL) and the actual polarization curve after the cell has been operational for some time, were used to analyze degradation of a PEM fuel cell exposed to voltage cycling as an accelerated stress test for electrocatalyst degradation, using methodology developed in the SAPPHIRE project [1].

The resulting polarization change curves are shown in Figure 12. The polarization change curves are close to straight lines so with linear regression it is possible to calculate the intercept on the y-axis and the slope of each curve. From the intercept on y-axis it is possible to calculate the loss of the ECSA, and from the slope the increase in resistance. The results are shown in Figure 13 and Figure 14. The loss of ECSA shows similar pattern to that measured independently by cyclic voltammetry (Figure 13). What is puzzling in that pattern is the loss of ECSA during the recovery period after 5000 cycles. This needs to be investigated further.

A majority of resistance increase during AST seems to be recoverable during both recovery periods after 5000 and 10000 cycles (Figure 14). It should be mentioned that high frequency resistance did not change during the AST, which is visible from EIS experiments (Figure 8-Figure 11). Also, the charge transfer resistance did not change during the AST (as it will be shown below) so the visible increase in resistance is almost solely due to the increase of resistance in the catalyst layer which degraded.
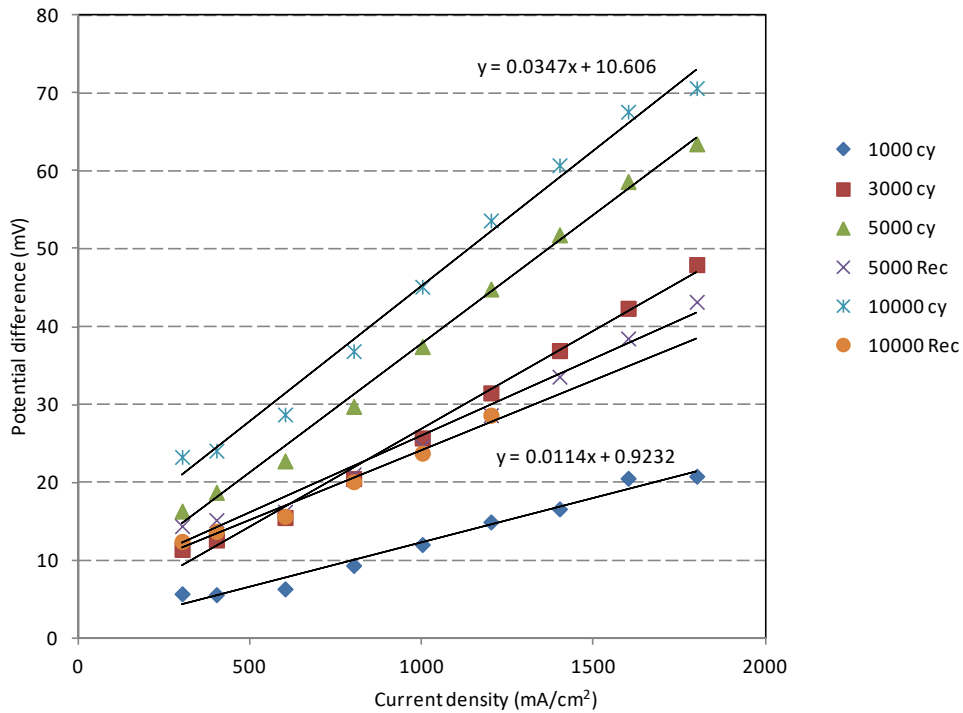
Figure 12: Polarization change curves resulting from polarization curves in Figure 3.
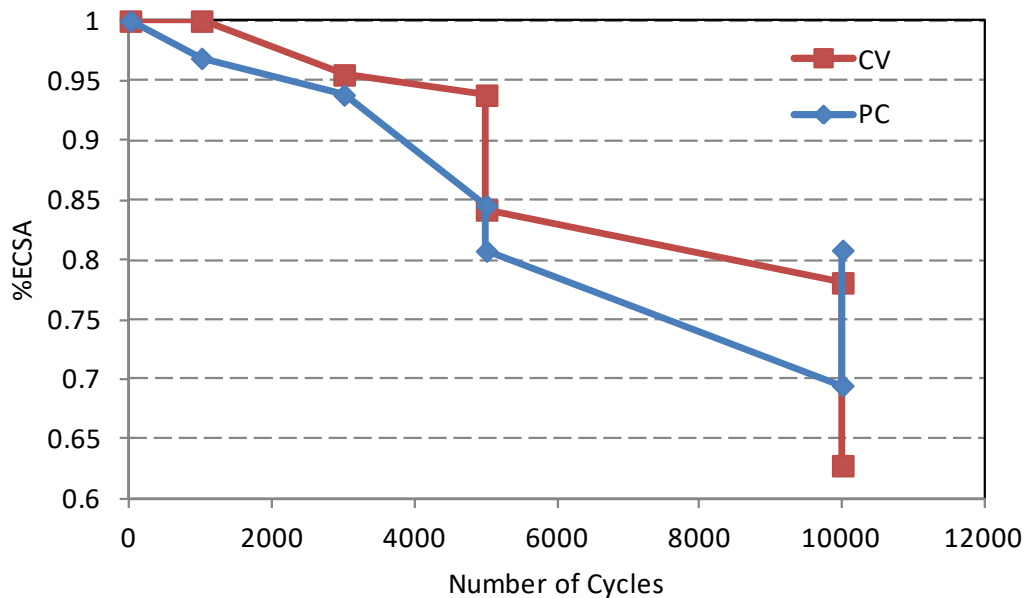

Figure 13: Comparison of the ECSA change during accelerated stress test calculated from cyclic voltammetry (CV) and those calculated from polarization change curves analysis (PC).
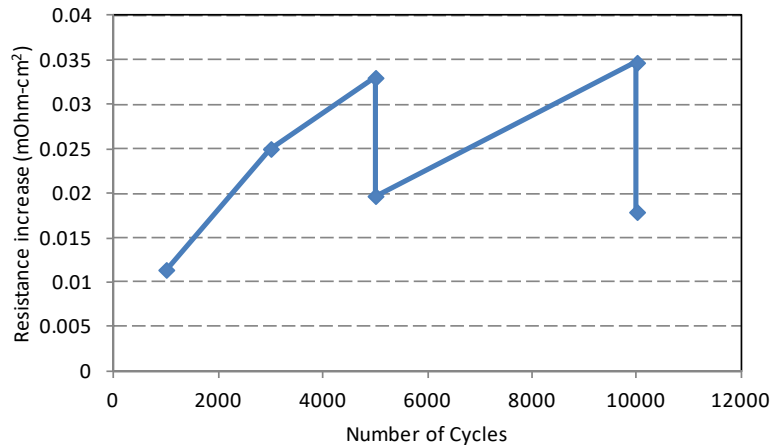
Figure 14: Resistance increase during accelerated stress test.

2.2.2 Application of 11-element impedance model to fuel cell degradation study

A novel equivalent circuit model of PEM fuel cell, consisting of 11 elements (Figure 15) was developed and validated by a series of experiments varying the operating conditions and current density [3]. This model originally developed to capture the processes that cause the low-frequency inductive loop in the impedance spectra [4] may be used as tool for further diagnostic purposes to identify the main degradation behaviors and their causes in order to define or improve suited control strategies in exploitation. Therefore, it has been applied here on the periodical impedance measurements to monitor performance degradation through the changes of model element values during the AST at three different current densities. The fit and numerical values of the model parameters for each impedance spectrum were estimated through the commercially available software ZView® 3.0 (Scribner Associates, Inc.), which is basically a least-square optimization procedure yielding the solution with the minimum sum of errors (differences between measured and calculated impedances for each of the frequencies) squared. The model elements of anode activation (R2 and C2) were held constant in the whole fitting procedure (anode activation is always present with a small contribution, but its diameter is completely independent of the current density and cathode catalyst degradation, as it is mainly related to the hydrogen oxidation reaction), while the other model elements were simultaneously fitted for every impedance spectra, successively for every step of the AST from the initial one at the BoL. In Figure 16, the model fitting results (light colored lines) are compared with the experimental EIS data (dark colored lines) at different current densities during the AST.
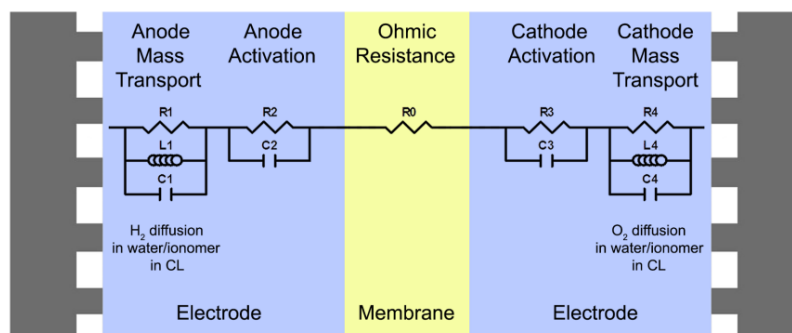
Figure 15: A novel 11-element equivalent circuit model that includes inductive behavior [3].
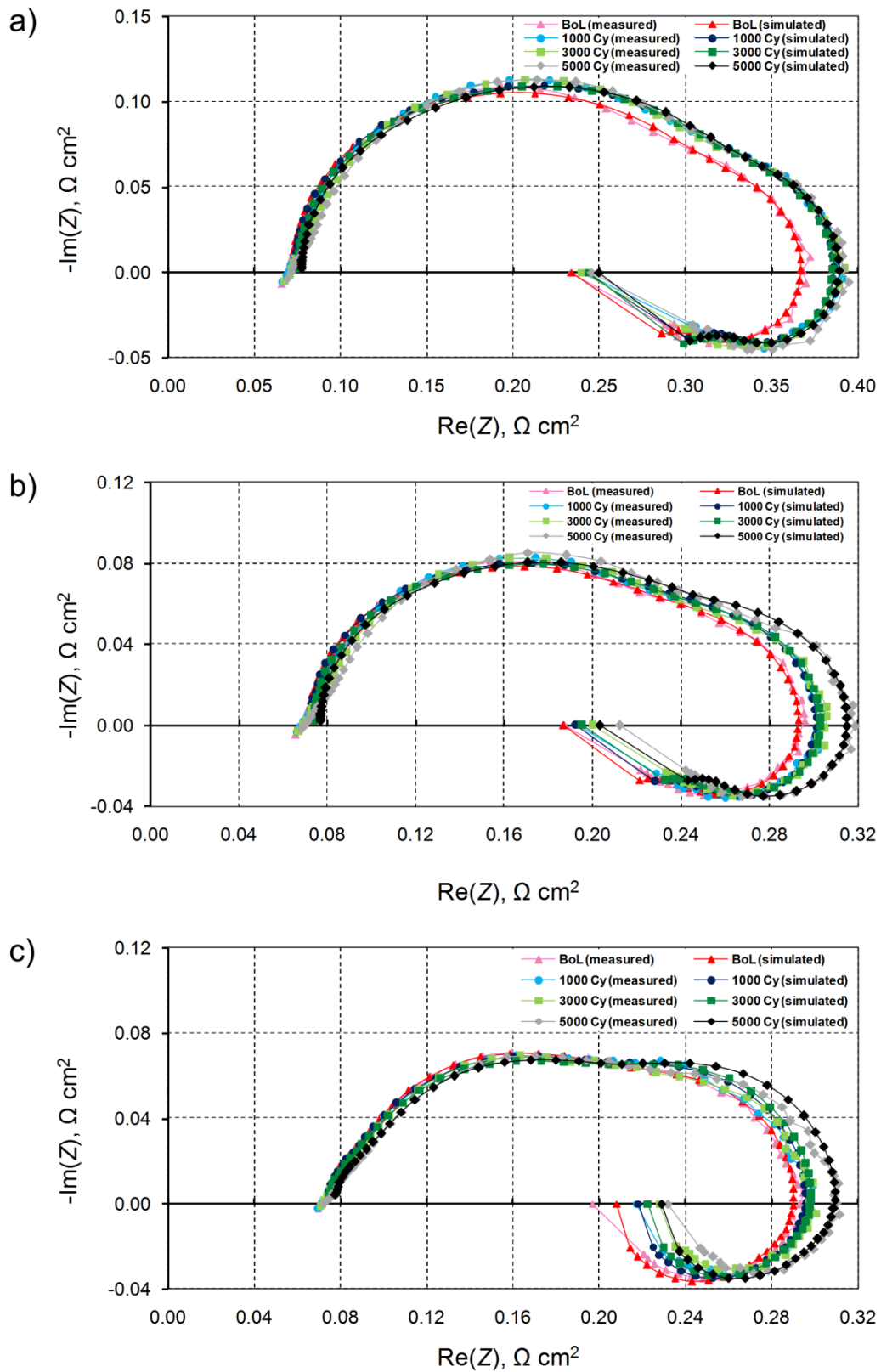
Figure 16: Comparison of measured and simulated impedance spectra during the accelerated stress test at: a) 0.3 A cm^{-2}; b) 0.6 A cm^{-2}; c) 1.2 A cm^{-2}.

As it can be seen in all of the Nyquist plots in Figure 16, a very good agreement between simulation and experimental data was achieved in the whole frequency range including the low-frequency capacitive loop followed by the inductive loop at every measured current density. Also, a good agreement between the slope of the steady-state polarization curves and the impedance extrapolated to zero perturbation frequency (DC point) was obtained.

As the trends of changes of model element values are very similar at different current densities, an influence of catalyst degradation on each extracted model element is given here only at 0.6 A cm^{-2} in Figure 17.
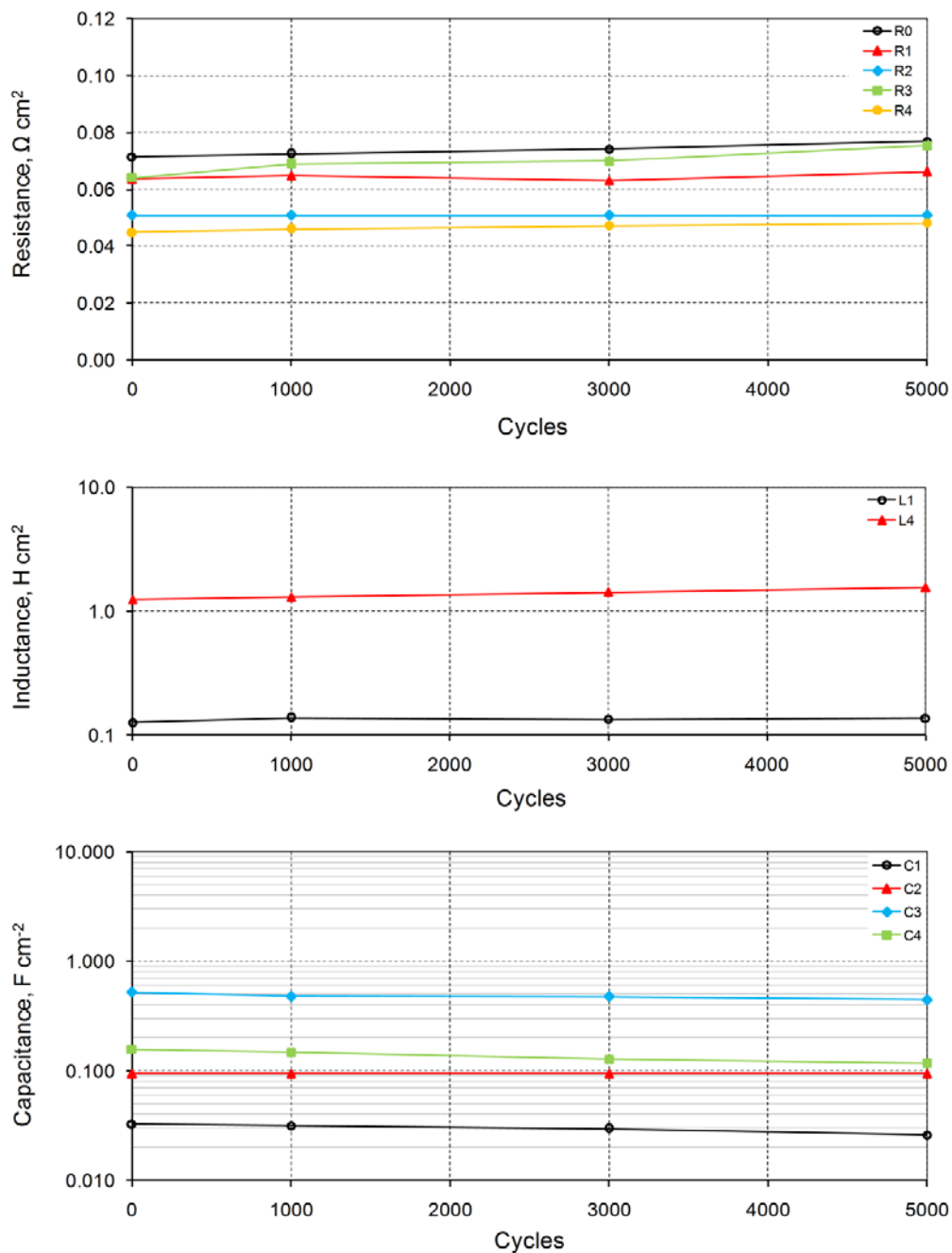
Figure 17: Changes of model element values at 0.6 A cm^{-2} during the accelerated stress test.

The results of the extracted model element values indicate that cathode catalyst layer resonant loop parameters (R4, L4 and C4) change the most during the accelerated stress test, also like the cathode charge transfer resistance (R3) and cathode double-layer capacitance (C3) that contribute to the cathode activation processes, which was expected as the target of the conducted AST was the cathode catalyst layer degradation due to loss of the ECSA, and this concurs also with the findings of the other diagnostic tests. As expected, cathode charge transfer resistance (R3) turns out larger than the anode charge transfer resistance (R2), because of slower kinetics of the oxygen reduction reaction (ORR), and it increased during the AST, also like the cathode catalyst layer resistance (R4). Therefore, the cathode catalyst layer capacitance (C4) significantly decreased during the AST, also like the cathode double-layer capacitance (C3). Cathode inductance (L4) is higher than the anode's (L1), probably because oxygen, as a bigger molecule than hydrogen, is more inert to dissolve in water or ionomer in the CL, and it increased significantly during the AST. The faster increase in the cathode inductance with the degradation would also be expected as the degradation test caused structural damage to the cathode CL, which should even further impede the oxygen absorption and dissolution process. Therefore, a higher inductance value can be an indicator of the increasing instability in cell operation (i.e. ECSA loss). The ohmic resistance (R0) also increased during the AST, as the EIS measurements were performed with not fully-hydrated reactants (83.4% RH). Changes of the anode catalyst layer resonant loop parameters (R1, L1 and C1) were either insignificant and/or probably within the error of the measurements and numerical methods involved in their calculation.

On the other hand, the low-frequency intercept (Total R) is the sum of all model resistors [3] and it shows a rising trend during the AST at every measured current density (Figure 18), but their overall values in the same point of AST are lower at higher current densities (of course, it can be stated only for this particular cell in the observed current density range). Also, the rising trends of the Total R during the AST are similar at all current densities, which can be an another sign of ECSA loss (e.g. voltage decay rates decrease with time and are almost constant at all current densities).
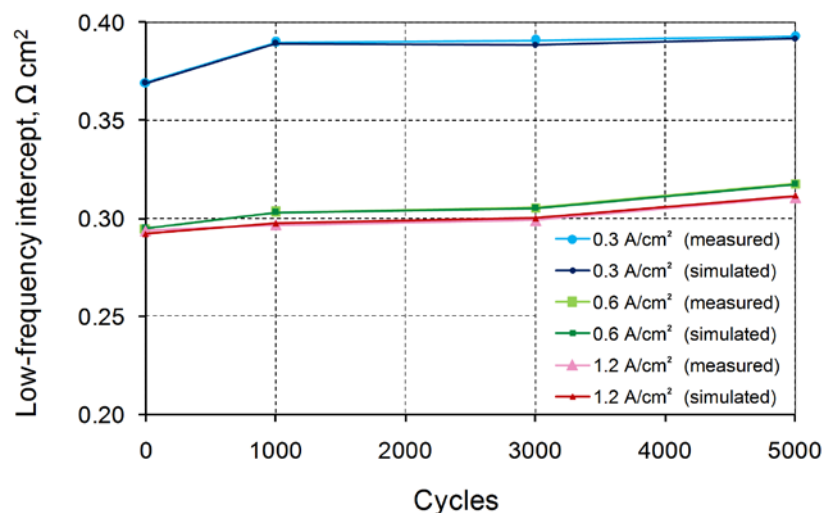

Figure 18. Comparison of measured and simulated low-frequency intercepts at different current densities during the accelerated stress test.

From the EIS experiments (Figure 18) it appears that the low frequency intercept, representing the sum of all resistances in a fuel cell equivalent circuit (thus it may be called the low frequency

resistance, LFR), may be used as an indication of fuel cell performance degradation due to catalyst layer degradation. Increase in resistance during the AST obtained by the polarization change curves analysis, basically represents the increase in the catalyst layer resistance. The difference between the resistance, R, obtained by fitting the polarization curves to equation:

$$V = V_o - b \ln (i/i_o) - iR$$

and the high frequency resistance (HFR) represents the catalyst layer resistance. It is noticeable from Figure 19 that it is the catalyst layer resistance that increased during the AST. HFR representing the membrane and other ohmic resistances did not change, and neither the charge transfer resistance (difference between dV/di and R) changed during the AST, thus leaving the catalyst layer resistance as the only resistance that changed (which is expectable because the AST was designed to degrade the catalyst layer). Why exactly the catalyst layer resistance increases during the AST remains to be explained, but it may be speculated that the AST caused certain morphological changes in the catalyst layer, which resulted in redistribution of the ionic and electronic pathways within the catalyst layer, thus resulting in increased resistance.
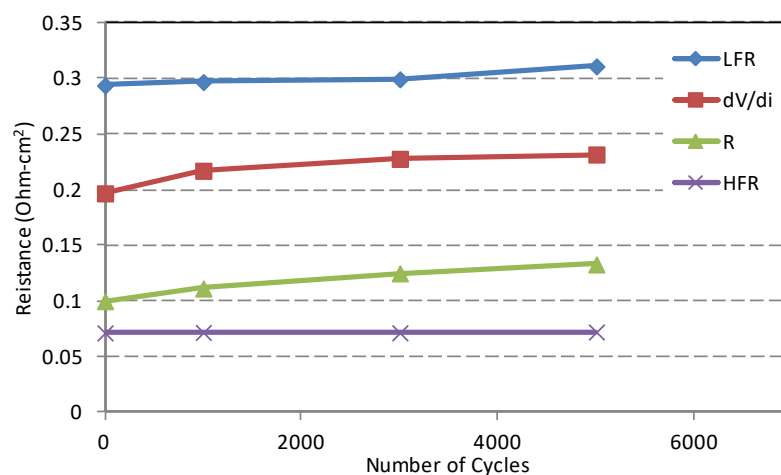
Figure 19: Change in resistance during the accelerated stress test.

2.2.3 A new direct measurement approach of low-frequency EIS intercept

From Figure 19 it seems that the LFR, as a sum of all the resistances, also includes the catalyst layer resistance, and therefore may be used as an indication of fuel cell performance degradation due to catalyst layer degradation.

In order to obtain the whole desired frequency range (down to 10 mHz), previously used measurement approach has to be repeated multiple of times, which is time consuming (cca. half an hour for every impedance spectra) and even inappropriate for on-line monitoring of real operational fuel cell system in practice. As the obtained impedance at the low-frequency intercept (i.e. Total R) is purely real and shows the most significant change with degradation, together with SINTEF who works on integration of diagnostics in the system control, we propose to develop a new on-line algorithm for direct impedance estimation, based on relay excitation feedback [5]. With this, it will be possible to find the appropriate frequency at intercept and calculate the impedance. The algorithm establishes a stable limit cycle oscillation with specified small amplitude and it will converge quite fast to the frequency with the desired phase properties of the impedance, in this case at the crossing

of the Nyquist curve and the real axis. The algorithm can be implemented in ordinary fuel cell control systems, eliminating the need for specialized EIS equipment. The actual frequencies that are in the ballpark of 0.1-10 Hz can easily be handled by standard measurement sampling rates without the need for special high-frequency data logging. Thus, catalyst degradation can be monitored without the need of measuring the whole EIS impedance spectrum and it will provide the possibility to determine the current state of the fuel cell from just one parameter value, which is very promising for the future implementation in the fuel cell control system. The direct identification approach will be further developed and tested in a fuel cell with known impedance properties in the continuation of this project.

2.3 Conclusions on fuel cell degradation diagnostics and future work

One of the main goals of the conducted experiments and further analysis was to get the first-hand experience on the catalyst degradation phenomena of the ElringKlinger's (single) PEM fuel cell during the AST consisting of frequent voltage cycling between 0.6 and 0.9 V. The observed fuel cell moderately degraded during the AST after 10000 cycles.

Polarization change curves analysis indicated slight loss of ECSA and slight increase in resistance. Also, they could not be explained at current densities lower than 300 mA cm^{-2} (probably due to constant flow rate/high stoichiometry).

The catalyst degradation was diagnosed with impedance periodical measurements taken during the AST at three different current densities and appropriate modeling, which yielded lower electrochemical activity in the electrodes visible through the EIS analysis as a mixture of increase in activation and mass transport losses. The applied 11-element impedance model managed to extract contributions of different phenomena responsible for the cell degradation, which were in accordance with the expected behavior, regarding their physical interpretations. The low-frequency intercept (Total R) increased most significantly during the AST with a rising and similar trend at every measured current density, whereas the membrane resistance increased only slightly. This concurs also with the findings (at least qualitatively) of the polarization change curves analysis and CV measurements, which indicated a slight loss of the ECSA caused by platinum dissolution due to intentionally frequent voltage cycling. The loss of the ECSA apparently resulted in structural changes within the CL, as the increase in mass transport in EIS suggests.

3 Implemented FCSAL diagnostic strategies

Franche-Comté University/FCLab contribution in WP1 is to develop diagnostic strategies to ensure the FC System Air Line (FCSAL) State-of-Health (SoH) monitoring. Three diagnostic strategies are implemented and validated on data gathered from previous FC LAB projects. They differ in the level of instrumentation required and the complexity of the analyzes / calculations to be carried out. In this work, the diagnostic approaches are based on data-driven diagnostic techniques. Algorithms are fed by physical signals such as stack voltage and pressure signal measurements. Guidelines for implementation of each strategy in the Giantleap project on data to be recorded on FCEB prototype from Bosch will be described.

3.1 Strategy Nr. 1: Diagnostic strategy based on stack voltage analysis

In order to achieve a fast and low-cost diagnostic, we propose a tool in which the FCSAL diagnostic is made by the observation of only one parameter – the stack voltage. The method adopted is based on the pointwise singularity analysis of the FC stack voltage, which is a typical non-linear signal. Actually, it is reasonable to assume that the operation of a FC under severe conditions affects the morphology of its voltage. The analysis of its local fluctuations can therefore provide direct information on the dynamics of the device and on its state-of-health as well. To perform a right characterization of these complex signals, some appropriate and robust techniques are obviously necessary.

We adopted morphological analysis of stack voltage based on wavelet leaders [6] in order to extract some latent information hidden in the signal and then to identify the signature of singularities for different fault operations. Indeed, the multifractal features can fully display the distribution of signal singularities, while the geometric characteristics and the local scaling behaviors are described more precisely. The developed diagnostic algorithm was tested and validated on rich databases built in the framework of FC LAB / UFC third party IFSTTAR previous projects.

3.1.1 Singularity Spectrum as a diagnostic tool

The singularity analysis, also named "multifractal analysis" allows the characterization of data by describing globally and geometrically the fluctuations of local regularity, usually measured by means of the Hölder exponent h. The numerical implementation of the mathematical formula basis of this method can be achieved using the wavelet leaders multifractal formalism. Detailed descriptions of the theoretical and practical relevance and benefits of the use of wavelet leaders for singularity analysis are depicted in [6-8].

3.1.2 FC diagnostic results and discussion

For the stack PEMFC$_{Auto}$, 10 scenarios are analyzed (normal and abnormal conditions including one fault or more complex situations with 2 or 3 faults occurred simultaneously). For the stack PEMFC$_{\mu CHP}$, 9 operating conditions (normal and abnormal conditions) are studied. In this aim, we use 30 voltage profiles for each FC operating condition; each voltage profile covers 1000 voltage samples acquired at a frequency f_s =11 Hz using the monitoring data system of the FC experimental test bench. Some examples of stack voltage signals recorded during various operating conditions corresponding to different fault scenarios are displayed in Figure 4.

The average SS computed using WLMA and related with the various faults shown in Figure 20 are plotted in Figure 21.
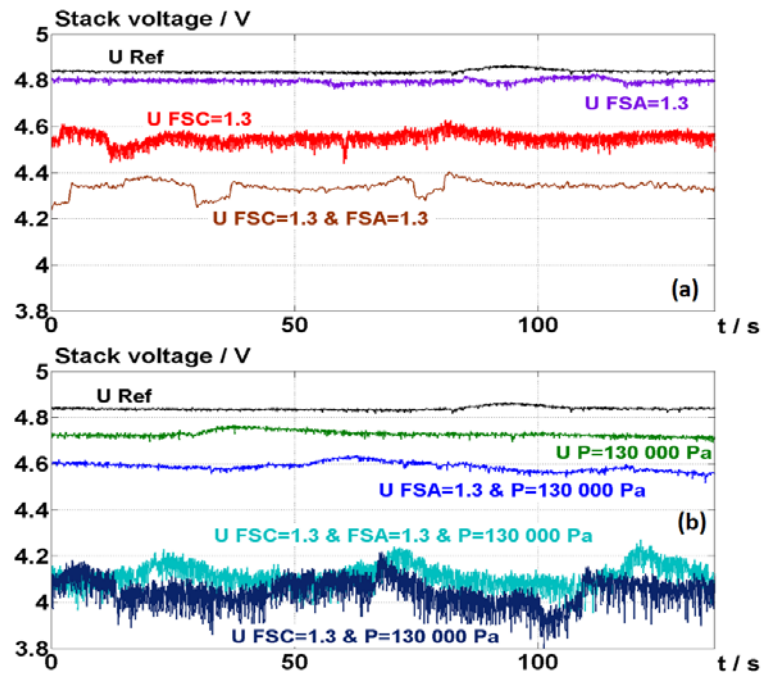
Figure 20: Examples of PEMFC stack voltages (V) vs. time acquired in different operating conditions.
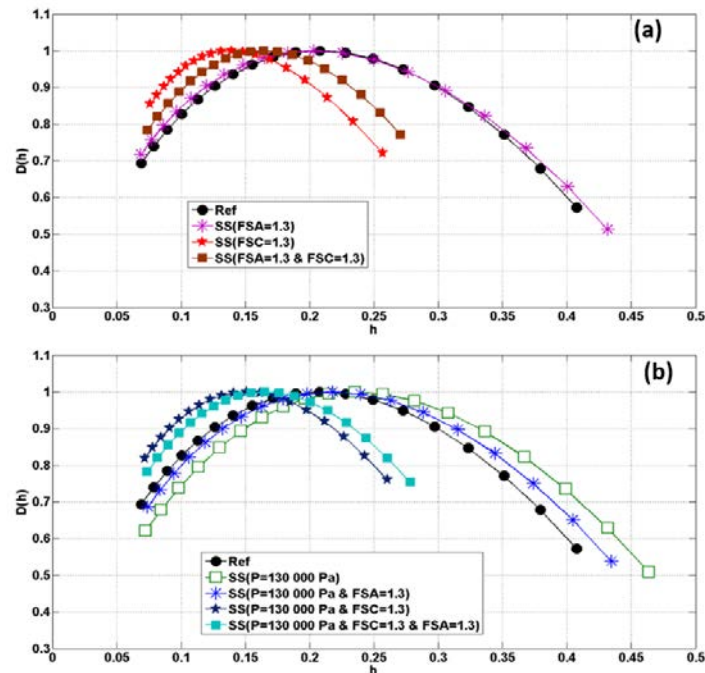
Figure 21: Average Singularity Spectra (SS) computed on 30 signals /operating conditions related with the different faults exhibited in Figure 20.

As we can see, each operating fault gives its own stamp on the stack voltage morphology. This behavior is revealed by the shape and the location of the corresponding singularity spectra (Figure 21). So, when the obtained SS is shifted to the left, that means a high irregularity of the voltage signal and conversely, when shifted to the right that reveals a more regular signal.

On one hand, the voltage signals associated to the FSC fault (single fault or combination of faults) contain sharp and impulsive variations (Figure 20) with relatively close magnitudes. This behavior is established by reduced singularity spectra (tiny concave arcs) and a high irregularity (Figure 21). On the other hand, large spectra are obtained with the FSA and P faults, which reveal the presence of several fluctuations sub-sets of points with various magnitudes on the voltage signals.

Based on these results, the classification of the obtained multifractal features is performed using Machine Learning approach named k Nearest Neighbors (kNN). The kNN are a non-parametric learning algorithm, which consists in assigning unlabeled features to the class of the most similar labeled examples. The similarity can be estimated by using Euclidean metric for example. To improve the performance of the fault classification method, the Minimum Redundancy - Maximum Relevance (MRMR) technique [9] is used to select some relevance features offering the best classification rates.

As we can see in Table 1 and Table 2, the proposed diagnostic strategy identifies successfully several complex operating faults (i.e, slight deflections from the nominal operating conditions. and even combination of faults) for both PEMFC$_{Auto}$ and PEMFC$_{\mu CHP}$. Especially. faults introduced in the FCSAL (cathode flow faults) are identified at 100% in the case of the two investigated FC stacks. These results will be published in International Journal of Hydrogen Energy and more details will be available in [8].

*Table 1: Confusion matrix of the good classification rates obtained with MRMR and kNN from the VSS computed with the stack voltage signals of the PEMFC$_{Auto}$. The studied FC operating conditions are: **Ref**: normal conditions - **DFSC**: cathode flow fault (slight air starvation) - **DFSA**: anode flow fault (slight H2 starvation) - **DP**: gas pressure fault (lower gas pressure) - **DT**: cooling circuit temperature fault (lower stack temperature) - **DCO**: carbon monoxide poisoning (H$_2$+CO).*

Class	C_0	C_1	C_2	C_3	C_4	C_5	C_6	C_7	C_8	C_9
Ref	**87.5**	0	0	12.5	0	0	0	0	0	0
DFSC	0	**100**	0	0	0	0	0	0	0	0
DFSA	0	0	**100**	0	0	0	0	0	0	0
DP	50	0	0	**50**	0	0	0	0	0	0
DT	0	0	0	0	**100**	0	0	0	0	0
DCO	0	0	0	0	0	**100**	0	0	0	0
DFSC & DP	0	0	0	0	0	0	**100**	0	0	0
DFSA & DP	0	0	0	0	0	0	0	**71.43**	28.57	0
DFSC & DFSA	0	0	0	0	0	0	0	0	**100**	0
DFSC & DFSA & DP	0	0	0	0	0	0	0	0	0	**100**

With: $C_0 \equiv \widehat{Ref}. C_1 \equiv \widehat{DFSC}. C_2 \equiv \widehat{DFSA}. C_3 \equiv \widehat{DP}. C_4 \equiv \widehat{DT}. C_5 \equiv \widehat{DCO}. C_6 \equiv \widehat{DFCS \& DP}.$

$C_7 \equiv \widehat{DFSA \& DP}. C_8 \equiv \widehat{DFSC \& DFSA}. C_9 \equiv DFSC \& \widehat{DFSA} \& DP.$

Table 2: Confusion matrix of the good classification rates obtained with MRMR and kNN from the VSS computed with the stack voltage signals of the PEMFC$_{\mu CHP}$. The studied FC operating conditions are: **Ref** *: normal conditions -* **DFSC↗**: *cathode flow fault (air over-supply) -* **DFSC↘**: *cathode flow fault (slight air starvation) -* **DFSA↗**: *anode flow fault (H$_2$ over-supply) -* **DFSA↘** *: anode flow fault (H$_2$ starvation) -* **DT↗**: *cooling circuit temperature fault (higher temperature) -* **DT↘** *: cooling circuit temperature fault (lower stack temperature) -* **DRH↗**: *gas dew point temperature fault (higher dew point temperatures) -* **DRH↘**: *gas dew point temperature fault (lower dew point temperatures).*

Class	C_0	C_1	C_2	C_3	C_4	C_5	C_6	C_7	C_8
Ref	**100**	0	0	0	0	0	0	0	0
DFSC↗	0	**100**	0	0	0	0	0	0	0
DFSC↘	0	0	**100**	0	0	0	0	0	0
DFSA↗	0	0	0	**90**	0	10	0	0	0
DFSA↘	0	0	0	0	**90**	0	0	0	10
DT↗	0	0	0	20	0	**80**	0	0	0
DT↘	0	0	0	0	0	0	**100**	0	0
DRH↗	0	0	0	0	0	0	0	**100**	0
DRH↘	0	0	0	0	0	0	0	0	**100**

With: $C_0 \equiv \widehat{Ref}$. $C_1 \equiv \widehat{DFSC↗}$. $C_2 \equiv \widehat{DFSC↘}$. $C_3 \equiv \widehat{DFSA↗}$. $C_4 \equiv \widehat{DFSA↘}$. $C_5 \equiv \widehat{DT↗}$. $C_6 \equiv \widehat{DT↘}$.

$C_7 \equiv \widehat{DRH↗}$. $C_8 \equiv \widehat{DRH↘}$.

3.1.3 Guidelines for implementing the diagnostic strategy in the Giantleap project

Figure 22 shows a simplified scheme of the FCSAL architecture developed for Giantleap project and coupled to the proposed diagnostic module based on strategy Nr. 1.
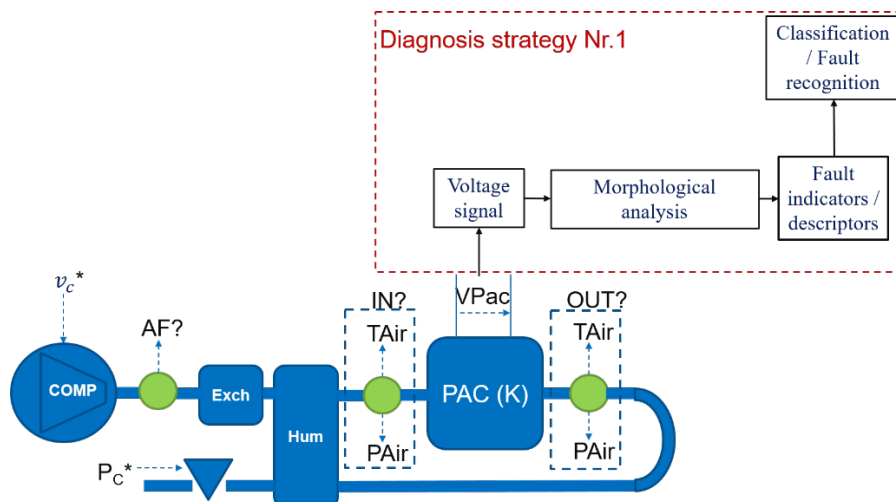

Figure 22: Simplified scheme of FCSAL coupled with the diagnostic module based on strategy Nr. 1.

Faults will be introduced in the air line side of the FC system prototype at Bosch facilities.

In this study, three FC operating scenarios will be investigated (viz. Ref., DFSC, and DP). Indeed, the failure scenarios will be experimented by the tuning of the auxiliary operating points to modify, namely: cathode stoichiometry factor 'FSC' and air pressure 'P'. The summary of the experimentations to be carried out on Bosch FC test bench is given in Table 3.

These tests duplicate faults, which are representative of any possible FCSAL dysfunctions. They include:

- Failure of the air supply system reflected by abnormal value of FSC parameter. This dysfunction may be related with a bad adjustment of the compressor speed, a compressor damage, a mass flow meter dysfunction, a control problem, flow-field channels obstruction by liquid water, etc.
- Failure of the air pressure, which can be caused by compressor dysfunction, back pressure valve damage, etc.

Collected PEMFC voltage signal data serve for supplying the developed diagnostic algorithm.

Table 3: Summary of experimentations to be carry out on Bosch FC test bench.

Parameters	Algorithm needs
Useful signal	Stack voltage
Sampling frequency	1 kHz
Voltage resolution	0.2 mV (16 bits)[*]
Operating conditions	Normal and abnormal
Changing Parameters	*1. Air stoichiometry rate* ➔ FC normal operation : $FSC_{air} = FSC_{nominal}$ ➔ FC abnormal operation : $FSC_{air} = FSC_{nominal} \pm 10\%$ $FSC_{air} = FSC_{nominal} \pm 20\%$ $FSC_{air} = FSC_{nominal} \pm 30\%$ *2. Air Inlet Pressure* ➔ FC normal operation : $P_{air} = P_{nominal}$ ➔ FC abnormal operation : $P_{air} = P_{nominal} \pm 10\%$ $P_{air} = P_{nominal} \pm 20\%$ $P_{air} = P_{nominal} \pm 30\%$
Additional parameters to be recorded	Inlet air temperature : T_{air} Stack temperature : T_{stack} H₂ stoichiometry rate: FSA_{H2}

[*] 0.2 mV (16 bits) for voltage and pressure signals (sensors outlet resolution) based on full scale measurement of 10 V.

3.2   Strategy Nr. 2: Diagnostic strategy based on signal analysis of inlet air pressure

We propose a tool in which the FCSAL diagnostic is made by the analysis of the FC inlet pressure sensor signal. The adopted method is based on statistical analysis combined with pattern recognition approach.

In order to elaborate the air pressure signal diagnostic strategy, a test bench has been developed in the FC platform in Belfort to emulate FCSAL. It includes the following components:

- compressor
- air mass flowmeter. BROOKS 5863S
- pneumatic back pressure valve
- pressure sensor KELLER PR 23S
- temperature sensor thermocouple type K.

The monitoring and the control of the FCSAL test-bench parameters are done through a National Instruments embedded controller and a dedicate control software developed with LabVIEW. In Figure 23, a picture of the developed test bench is shown. It is dedicated to compressor flow range up to 300Nl/min and 3b pressure.
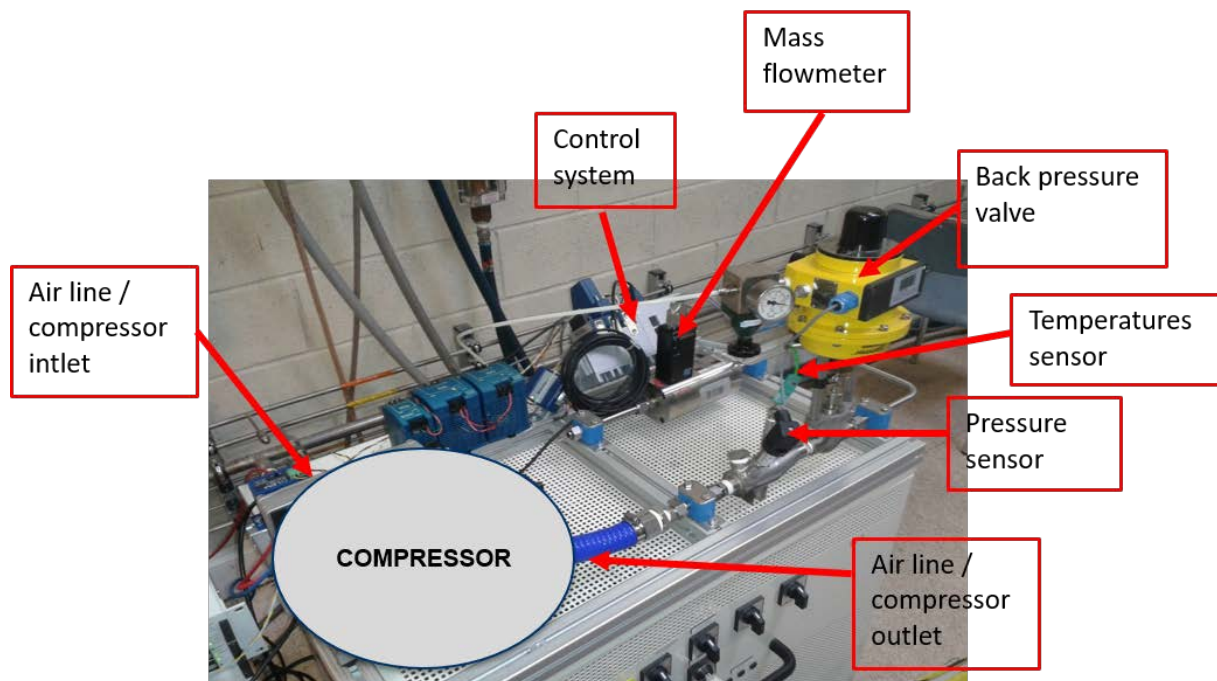

Figure 23: Air compressor test bench from UFC (FC LAB).

In this study, four air line operating scenarios are investigated. The introduced fault scenarios are considered as common occurred faults in the air line part of a FC system. In the case of the Normal Operation (NO) scenario, air line ancillaries operate without any failure (no fault is introduced). In the case of the three other operating scenarios, faults are introduced and are related to the following air line dysfunctions:

- Compressor Speed Control Faults (CSCF): a drop in the compressor speed set point is voluntary caused.

- Air Leakage Fault (ALF): an air leakage is deliberately caused by opening partially a dedicated valve in the air duct.
- Inlet Air Fault (IAF): in this test, the air line inlet of the compressor is partially clogged.

The pressure signal is recorded for the four experimentations, with a sampling frequency f_s = 1 kHz. The data serve to supply the diagnostic algorithm based on the statistical analysis.

3.2.1 Statistical analysis of pressure signal combined with kNN

The diagnostic strategy is based on the statistical analysis of the recorded pressure signals during the experimentation and carried out for the four operating scenarios. The first step of the algorithm includes feature extraction. Feature extraction is the process of defining a set of features, which will most efficiently or meaningfully represent the information that is important for analysis and classification. Indeed, first order statistics or moments of the pressure signal are computed on a scanning window, such as:

- *Maximum* and *Minimum* values of the pressure amplitude.
- *Mean* value of the pressure.
- *Variance* of pressure samples.
- *Kurtosis* of the signal. *Kurtosis* is used for describing or estimating a distribution's peakedness and frequency of extreme values.
- *Skewness* of the signal. *Skewness* is a measure of the asymmetry of the pressure data around the mean sample.

The plots of the statistical features estimated on the pressure signal by applying a scanning window size of 500 samples are given in Figure 24.
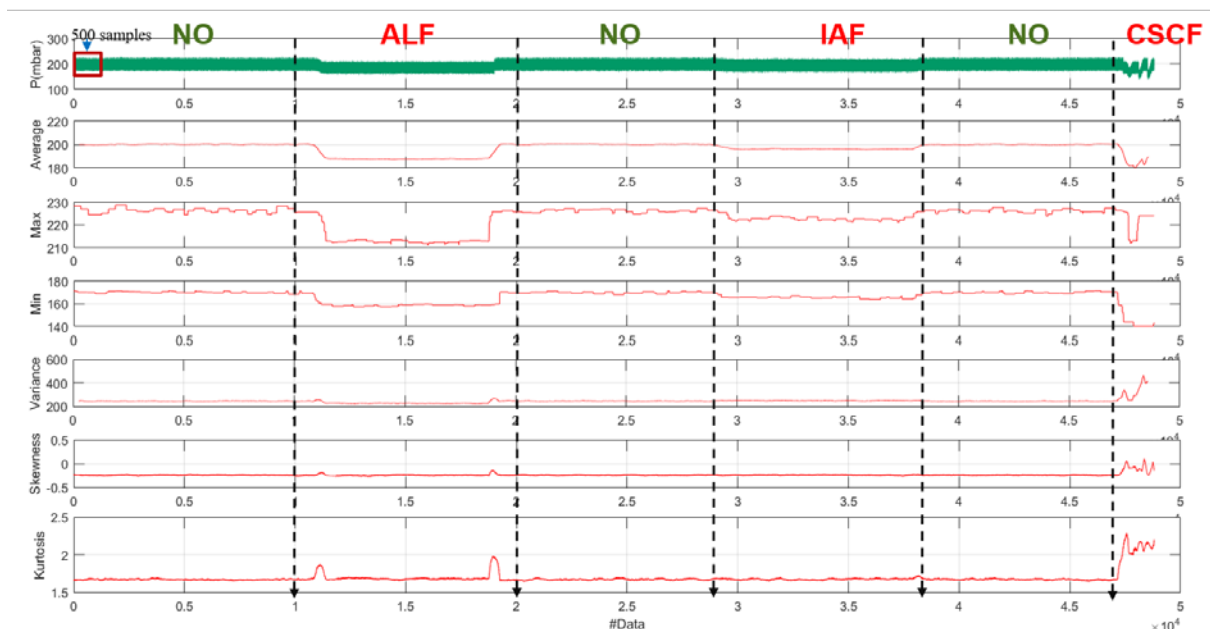

Figure 24: Plots of statistical features estimated on an example of pressure signal for the four investigated operating scenarios of a FCSAL. Applied scanning window size = 500 samples.

The second step of the algorithm applies pattern recognition approach, called k-Nearest Neighbors (kNN), in order to separate the studied operating scenarios into four classes, namely. NO class, CSCF class, ALF class and IAF class. Figure 25 illustrates the principle steps of the elaborated diagnostic strategy.
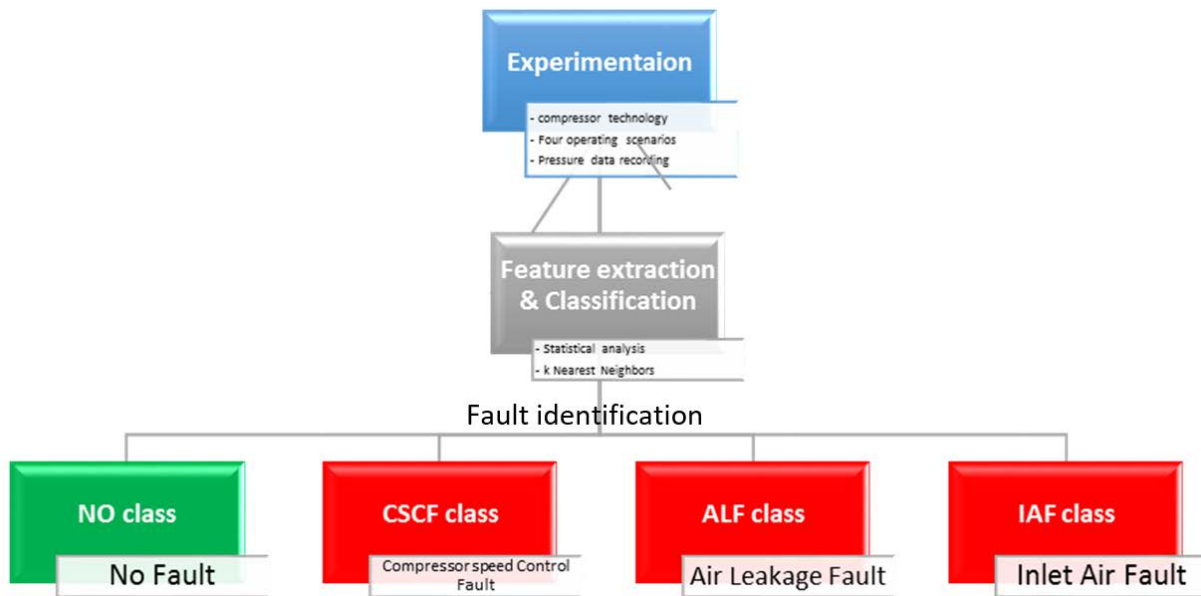

Figure 25: Steps of the diagnosis strategy based on statistical analysis combined with kNN of pressure data.

3.2.2 Diagnostic results and discussion

We assess a performance of the proposed algorithm by applying it to the collected pressure data. kNN is a supervised classification method, the classification algorithm is organized in two phases: a training phase and a test one. Actually, a matrix of 500 observations × 6 descriptors is used to generate a training database and a matrix of 200 new observations × 6 descriptors serves as a test data.

The confusion matrix of the best results obtained on each class thanks to a scanning window size of 500 samples is shown in Table 4.

Table 4: Confusion matrix of the good classification rate (%), obtained for the 4 classes.

Class	NO	ALF	IAF	CSCF
NO	100	0	0	0
ALF	0	100	0	0
IAF	0	0	100	0
CSCF	0	0	0	100

Number of class = 4.
Training set = 500 observations.
Test set = 200 new observations.
Number of statistical descriptors = 6.
Scanning window size = 500 samples.
Computing time = 1.24 seconds for both training and test steps.

3.2.3 Guidelines for implementing the diagnostic strategy in the Giantleap project

Figure 26 shows a simplified scheme of the FCSAL architecture developed for Giantleap project and coupled to the proposed diagnostic module based on strategy Nr. 2.
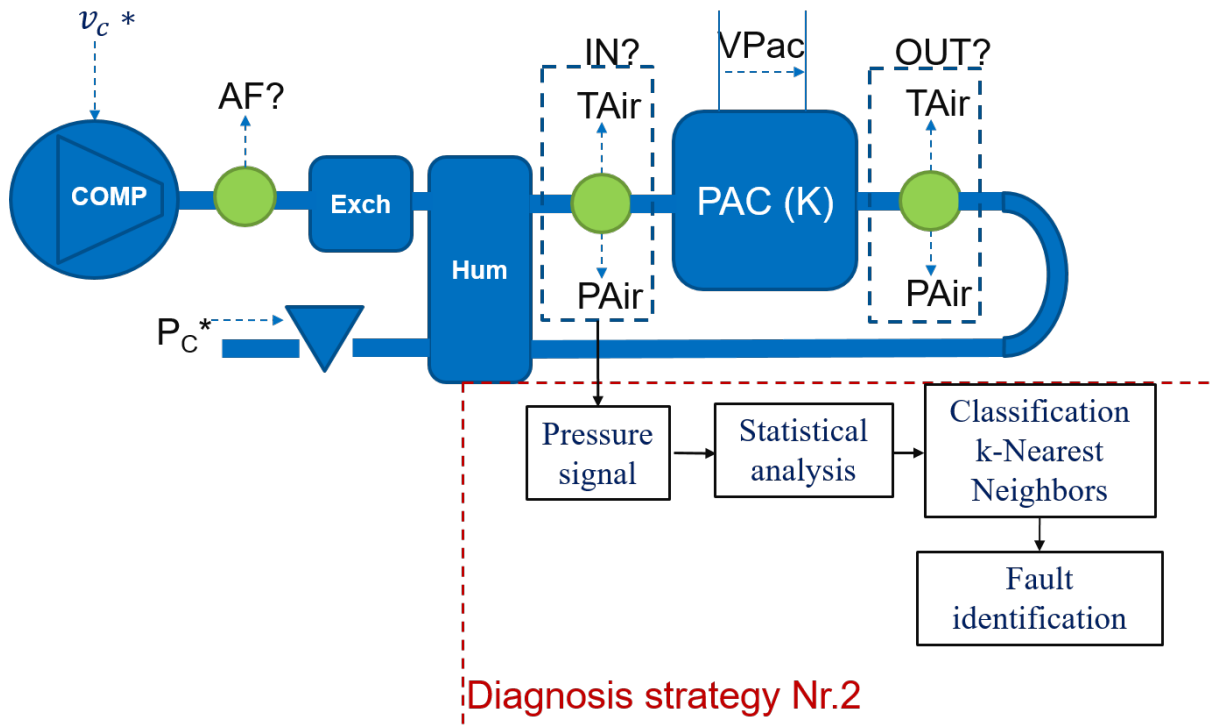

Figure 26: Simplified scheme of FCSAL coupled with the diagnostic module based on strategy Nr. 2.

Experimentations of air leakage fault, control compressor speed and inlet air partially clogged will be carried out from experimentations on the FC system prototype at Bosch facilities. Collected pressure data will feed the implemented diagnostic algorithm for validation.

3.3 Strategy Nr. 3: Diagnostic strategy based on compressor speed estimation

In the last diagnostic strategy, the work is devoted to implement a law that estimates the compressor speed from pressure data measurements.

A compressor technology is experimented using a test bench shown in Figure 23, for different pressure (in mbar) and Air Flow (AF in Nl/min) values. Some examples of AF and pressure data recorded with fs = 1 kHz are given in Figure 27. During the experimentation, AF value is kept stable while P varies of about five stages. The higher speed of the experimented compressor technology reaches 1500 rpm.
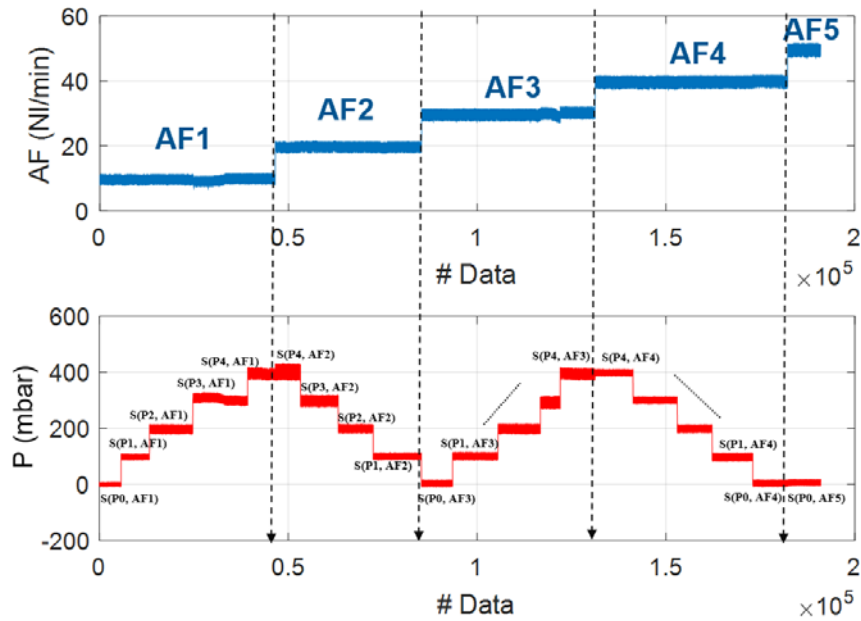
Figure 27: Typical curves of AF and P data recorded during a compressor experimentation.

3.3.1 Compressor speed estimation

Pressure data gathered during the experimentation are analyzed in the frequency domain. Spectral analysis is performed in order to estimate the frequency signature described by the fundamental and the harmonics containing in the signal.

Estimates of fundamental, 2nd and 3rd harmonics for different pairs (AF, P) values are plotted in Figure 28. Results show an increase tendency of frequency components according to AF and P amplitudes.

Detailed values of frequency components are incorporated to the experimental design garnered from the experimentation phase (see Table 5).
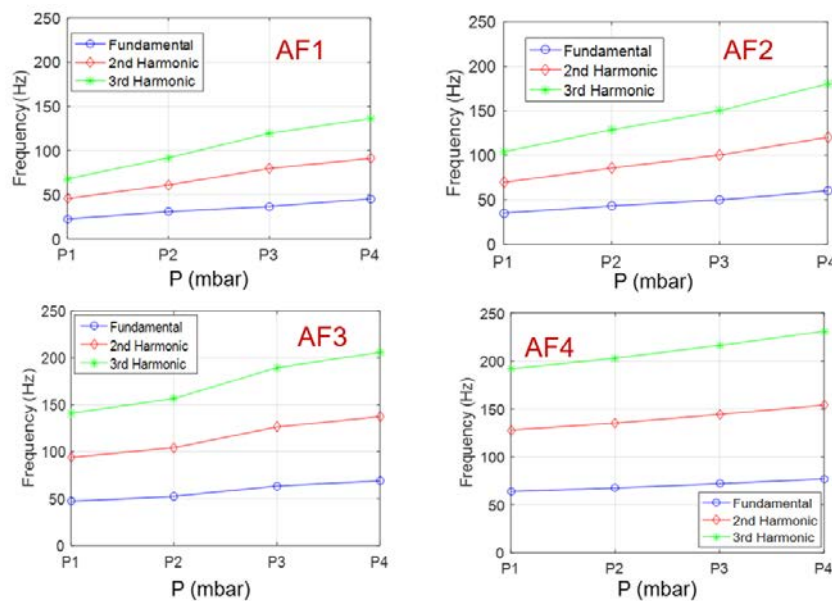

Figure 28: Typical curves of frequency components according to P amplitude, for different AF values.

As one can see in the last column of Table 5, an average error of 13 rpm is computed between the set point of the compressor speed v_c and the estimated value v_e.

Table 5: Frequency signatures for different pairs (AF, P).

| Air Flows (Nl/min)	Pressure (mbars)	Fundamental F (Hz)	Fundamental magnitude (db)	2nd harmonic	3rd harmonic	Compressor velocity v_c (rpm)	Estimated v_e (rpm)	Error v_e- v_c
AF1 = 10.02 Control = 10	P1 = 99.48	22.66	8.42	45.67	68.00	330.00	339.90	9.90
	P2 = 198.11	30.66	11.68	61.00	91.66	450.00	459.90	9.90
	P3 = 305.37	36.66	15.69	79.66	119.33	594.00	549.90	-44.10
	P4 = 395.61	45.33	18.65	91.00	136.33	673.00	679.95	6.95
AF2 = 20.02 Control = 20	P1 = 100.27	35.00	9.00	69.67	104.00	516.00	525.00	9.00
	P2 = 199.35	43.00	14.99	85.66	128.66	639.00	645.00	6.00
	P3 = 300.09	50.00	19.45	100.33	150.33	753.00	750.00	-3.00
	P4 = 402.83	60.00	23.12	120.33	180.33	900.00	900.00	0.00
AF3 = 30.09 Control = 30	P1 = 100.40	47.00	15.36	94.00	141.00	703.00	705.00	2.00
	P2 = 183.24	52.33	16.87	104.33	156.66	781.00	784.95	3.95
	P3 = 293.71	63.33	19.69	126.33	189.66	945.00	949.95	4.95
	P4 = 397.34	68.66	17.26	137.33	206.00	1034.00	1029.9	-4.10
AF4 = 40.15 Control = 40	P1 = 106.77	64.00	15.83	128.00	192.00	885.00	960.00	75.00
	P2 = 199.65	67.66	14.89	135.53	203.00	1012.00	1014.90	2.90
	P3 = 308.52	72.00	13.02	144.33	216.33	1055.00	1080.00	25.00
	P4 = 398.78	77.00	11.85	154.00	231.00	1090.00	1155.00	65.00
AF5 = 49.67 Control = 50	P = 7.03	76.66	12.39	153.33	230.00	1097.00		
							1149.90	52.90
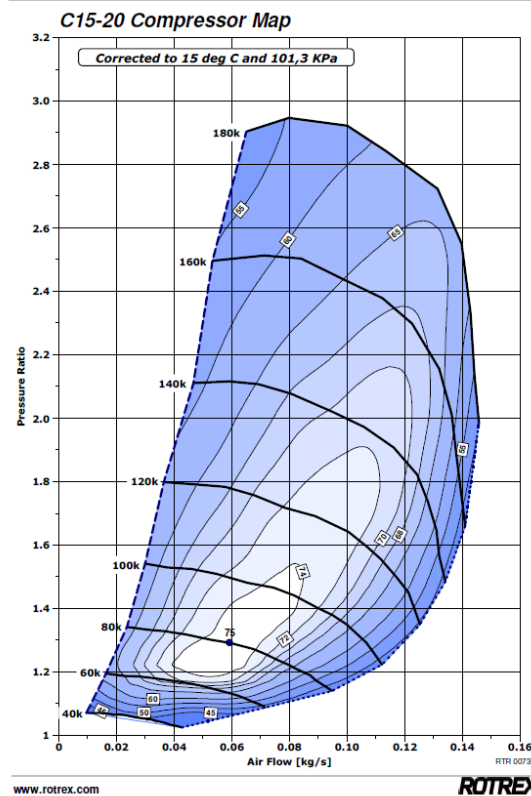
Figure 29: Compressor map of the implemented compressor in the FCEB prototype.

3.3.2 Guidelines for implementing the diagnostic strategy in the Giantleap project

The main idea of the diagnostic strategy is to compare the value of the compressor speed estimated for each pair (AF, P) to a reference lookup table. In this study, the lookup table is the C15-20 compressor map given in Figure 29. In FCEB application, the compressor speed can exceed 120,000 rpm. In this case, the acquisition frequency needed for the algorithm operation is at least 10 kHz.

Figure 30 shows a simplified scheme of the FCSAL architecture in the FCEB from VDL, coupled to the diagnostic module based on strategy Nr. 3.
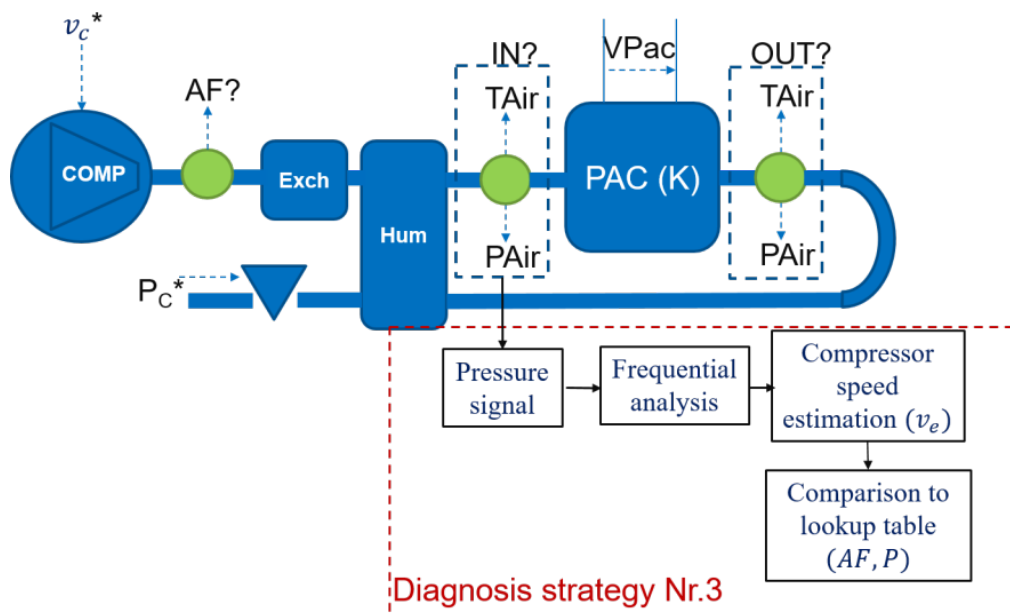

Figure 30: Simplified scheme of the FCSAL coupled with the diagnostic module based on strategy Nr. 3.

3.4 Summary of proposed diagnostic strategies

- Diagnostic strategy Nr. 1
  - ✓ Based on the stack voltage analysis.
  - ✓ Already applied successfully in the framework of previous projects (implemented in Matlab environment).
  - ✓ Strategy validation on Bosch system data is pending.

- Diagnostic strategy Nr. 2
  - ✓ Based on the inlet pressure signal analysis.
  - ✓ Strategy tested with success in compressor experiments conducted at FC LAB.
  - ✓ Strategy validation on Bosch system data is pending.

- Diagnostic strategy Nr. 3
  - ✓ Based on the compressor speed estimation.
  - ✓ Strategy tested on two compressor technologies at FC LAB.
  - ✓ Validation on Bosch system data probably difficult due to the needs of the developed algorithm (ex. high sampling frequency = up to 10 kHz).

4   References

[1] Bezmalinovic, D., Simic, B., Barbir, F., Characterization of PEM fuel cell degradation by polarization change curves, Journal of Power Sources, Volume 294, 2015, pp. 82–87.

[2] Garland, N., Benjamin, T., Kopasz, J., DOE Fuel Cell Program: Durability Technical Targets and Testing Protocols, ECS Transactions, Volume 11, 2007, pp. 923-931.

[3] Pivac, I., Šimić, B., Barbir, F., Experimental diagnostics and modeling of inductive phenomena at low frequencies in impedance spectra of proton exchange membrane fuel cells, Journal of Power Sources, Volume 365, 2017, pp. 240–248.

[4] Pivac, I., Barbir, F., Inductive phenomena at low frequencies in impedance spectra of proton exchange membrane fuel cells – A review, Journal of Power Sources, Volume 326, 2016, pp. 112–119.

[5] Pivac, I., Halverson I. J., Bezmalinović, D., Barbir, F., Zenith F., Low-frequency EIS intercept as a diagnostic tool for PEM fuel cells degradation, 7th European Fuel Cell Technology & Applications Conference - Piero Lunghi Conference, Naples, Italy, December 12-15, 2017

[6] Benouioua, D., Candusso, D., Harel. F., Oukhellou, L., Multifractal analysis of stack voltage based on wavelet leaders: a new tool for the on-line diagnosis of PEMFC, Fuel Cells Journal, Volume 17, Issue 2, 2017, pp. 217-224.

[7] Benouioua, D., Candusso, D., Harel. F., Oukhellou, L., The dynamic multifractality in PEMFC stack voltage signal as a tool for the aging monitoring, International Journal of Hydrogen Energy, Volume 42, Issue 2, 2017, pp. 1466-1471.

[8] Benouioua, D., Candusso, D., Harel. F., Picard., P., François, X., On the issue of the PEMFC operating fault identification: generic analysis tool based on voltage pointwise singularity strengths, International Journal of Hydrogen Energy, Vol. x. Issue x. 2017 (Preprint)

[9] Hanchuan Peng's web site. Information on mRMR (minimum Redundancy Maximum Relevance Feature Selection). Web site: http://home.penglab.com/proj/mRMR/ 2017.